

pubs.acs.org/est Article

Description of Dissolved Organic Matter Transformational Networks at the Molecular Level

Dennys Leyva, Muhammad Usman Tariq, Rudolf Jaffé, Fahad Saeed, and Francisco Fernandez-Lima*



Cite This: Environ. Sci. Technol. 2023, 57, 2672–2681



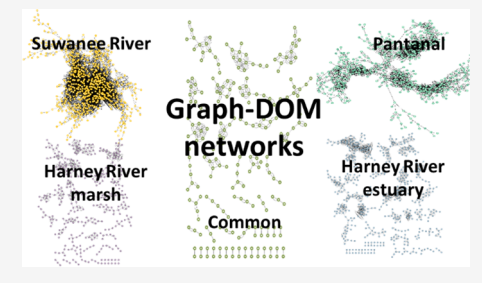
ACCESS

III Metrics & More

Article Recommendations

Supporting Information

ABSTRACT: Dissolved Organic Matter (DOM) is an important component of the global carbon cycle. Unscrambling the structural footprint of DOM is key to understand its biogeochemical transformations at the mechanistic level. Although numerous studies have improved our knowledge of DOM chemical makeup, its three-dimensional picture remains largely unrevealed. In this work, we compare four solid phase extracted (SPE) DOM samples from three different freshwater ecosystems using high resolution mobility and ultrahigh-resolution Fourier transform ion cyclotron resonance tandem mass spectrometry (FT-ICR MS/MS). Structural families were identified based on neutral losses at the level of nominal mass using continuous accumulation of selected ions-collision induced dissociation (CASI-



CID)FT-ICR MS/MS. Comparison of the structural families indicated dissimilarities in the structural footprint of this sample set. The structural family representation using Cytoscape software revealed characteristic clustering patterns among the DOM samples, thus confirming clear differences at the structural level (Only 10% is common across the four samples.). The analysis at the level of neutral loss-based functionalities suggests that hydration and carboxylation are ubiquitous transformational processes across the three ecosystems. In contrast, transformation mechanisms involving methoxy moieties may be constrained in estuarine systems due to extensive upstream lignin biodegradation. The inclusion of the isomeric content (mobility measurements at the level of chemical formula) in the structural family description suggests that additional transformation pathways and/or source variations are possible and account for the dissimilarities observed. While the structural character of more and diverse types of DOM samples needs to be assessed and added to this database, the results presented here demonstrate that Graph-DOM is a powerful tool capable of providing novel information on the DOM chemical footprint, based on structural interconnections of precursor molecules generated by fragmentation pathways and collisional cross sections.

KEYWORDS: DOM, FT-ICR CASI-CID MS/MS, TIMS-FT-ICR MS, structural family, network

1. INTRODUCTION

Dissolved Organic Matter (DOM) is an extremely complex mixture of organic species with a wide variety of chemical signatures and is considered a fundamental component of the biogeochemical global carbon cycle. 1-6 Due to its crucial role in aquatic ecosystems, the characterization of dissolved organic matter (DOM) across different environments has been the focus of numerous studies⁷⁻¹⁶ and can be classified in (i) bulkand (ii) molecular-level characterizations. 10,17-20 The molecular-level characterization is gaining primary attention because of the increasing need to better understand how changes in DOM makeup across environments affect critical ecological processes (e.g., the global carbon cycle). 4,21 The introduction of ultrahigh-resolution mass spectrometry (e.g., Fourier transform ion cyclotron mass spectrometry, FT-ICR MS) has significantly advanced our understanding of the DOM molecular makeup. 18,22 Improvements in dynamic range, signal-to-noise ratio, ultrahigh mass resolving power, mass accuracy, and mass selection have distinguished FT-ICR MS as a unique technique for the analysis of complex mixtures.^{23,24} For example, several thousand chemical components distributed across various heteroatom classes can be now routinely identified at a sub ppm error level from DOM samples in a single broadband FT-ICR MS analysis. ^{25–27}

However, the structural characterization of DOM remains a significant challenge. The high chemical diversity and high isomeric complexity has significantly limited the DOM structural characterization. Traditional NMR studies are limited by the need of pure and relative high concentrations of purified components. (e.g., liquid chromatography approach, chromatographic (e.g., liquid chromatography and gasphase separations (e.g., ion mobility 12,27,34–36 and ultrahighresolution FT MS 13,18,37–39) have been explored. Most of the studies attempting to gain DOM structural information have relied on identifying structural classes by NMR (i.e., aliphatic,

Received: July 1, 2022 Revised: January 18, 2023

Accepted: January 18, 2023 Published: February 1, 2023





aromatic, olefinic, etc.) ^{28,29,40} and functional groups from tandem mass spectrometry (i.e., carboxylic moiety from $\rm CO_2$ neutral loss). ^{41–43}

A fundamental aspect for the structural DOM characterization is the need to separate and identify isomeric components, as well as to better understand the DOM transformation pathways. 11,33 In 2020, trapped ion mobility spectrometry (TIMS) coupled to FT-ICR MS⁴⁴ allowed for the first time isomeric separation followed by chemical formula level fragmentation of a DOM sample, and potential isomeric structures were proposed. The integration of a score system from in silico MS/MS fragmentation and structural screening based on experimental vs theoretical ion-neutral collisional cross sections (CCS) allowed for a structural assignment with reduced ambiguities. Despite the unique advantages of this methodology, its application to a large-scale study (e.g., thousands of chemical formulas) could be challenging and ultimately impractical for routine characterization. In 2022, a more feasible approach based on the neutral loss patterns of nominal mass isolated precursors using continuous accumulation of selected ions (CASI) followed by collision induced dissociation (CID) and FT-ICR MS detection⁴⁵ was proposed. Over 1000 structural families of DOM related components from 110 nominal masses were identified in an SPE-DOM sample from the Pantanal wetland, Brazil. When combined with a novel visualization approach based on a Cytoscape network (Graph-DOM^{45,46}), the structurally interconnected DOM families were visualized, and potential biogeochemical transformation processes were identified.

In the present work, we further interrogate the DOM structural space by identifying the transformational networks common to different DOM samples. In particular, we implement for the first time a comparison across DOMs based on isomeric mobility separation and neutral loss-based MS/MS fragmentation strategies for the identification of common and unique structural families. This unsupervised structural classification workflow allows for the structural footprint across aquatic DOMs. Examples are shown for the case of SPE-DOM samples from a Suwannee River fulvic acid standard (SRFA), a wetland sample from Brazil (Pantanal), and two end-member samples from a marsh-to-estuary transect in the Harnery River (Florida Everglades; HR-1 and HR-5).

2. EXPERIMENTAL SECTION

Sample Preparation. DOM samples from four aquatic environments were studied: Suwanee River Fulvic Acid (SRFA), a wetland from Brazil (Pantanal), and HR-1 and HR-5 from a marsh-to-estuary transect on the Harney River (Florida Everglades). A Suwanee River Fulvic Acid standard was obtained from the International Humic Substances Society (IHSS, http://humic-substances.org). The SRFA stock solution (1 mg/mL) was prepared by dissolving 1 mg of SRFA standard powder in 1 mL of methanol. Pantanal (Pantanal National Park, Brazil) and HR-1 and HR-5 (Harney River, Florida Everglades) were obtained by solid phase extraction (SPE) of surface water. Details of the sampling protocol and the SPE method used are described elsewhere. 9,47,48 Briefly, one liter of water was collected using precleaned plastic bottles and filtered using GFF precombusted $0.7~\mu m$ glass fiber filters no later than 6 h after collection. For the SPE procedure, samples were acidified (pH 2) and loaded onto a 1 g Bond Elut PPL cartridge (Agilent, Santa Clara, CA, USA) conditioned with 1 cartridge volume of methanol

followed by 1 cartridge volume of pH 2 Milli-Q water. The loaded PPL cartridge was then rinsed with pH 2 Milli-Q water for desalting and dried under a nitrogen gas flow for 5 min, before the elution of DOM components with 20 mL of methanol. SPE-DOM extracts were stored at $-20\,^{\circ}$ C in amber glass vials until further analysis. All DOM samples were diluted in denatured ethanol to infuse a similar DOM concentration (\sim 5 mg/L). All solvents (Optima LC-MS grade) were obtained from Fisher Scientific (Pittsburgh, PA).

(-)ESI-FT-ICR MS. A SolariX 9T ESI-FT-ICR MS spectrometer (Bruker Daltonics, MA) equipped with an infinity ICR cell was optimized for high transmission of ions in the $100-1200 \, m/z$ range. Diluted DOM samples were ionized using an electrospray ionization source (Apollo II ESI design, Bruker Daltonics, Inc., MA) in negative ion mode and injected at 200 µL/h. Typical operating conditions were 3700-4200 V capillary voltage, 4 L/min dry gas flow rate, 1.0 bar nebulizer gas pressure, and a dry gas temperature of 200 °C. Operational parameters were as follows: funnel rf amplitude 160 voltage peak-to-peak (Vpp), capillary exit -150 V, deflector plate -140 V, skimmer1 -20 V, transfer line RF 350 Vpp, octupole RF amplitude 350 Vpp, and collision cell RF 1100 Vpp. An Agilent ESI-L low concentration Tuning Mix calibration standard (Agilent, Santa Clara, CA, USA) was used during the instrument tuning. Broadband MS₁ spectra (200 coadded scans) of the four DOM samples were collected at 4 MW data acquisition size (mass resolution of ~ 300 k at 400 m/z).

(–)ESI-FT-ICR CASI CID MS/MS. Comprehensive MS/MS data of SRFA, Pantanal, HR-1, and HR-5 DOM samples were obtained by performing ESI-FT-ICR CASI CID MS/MS (see details in ref 45). Briefly, odd mass ions (m/z range 261–477), sequentially isolated in the quadrupole at nominal mass, were accumulated for 5-7 s in the collision cell and further subjected to CID before analysis in the ICR cell. Tailored CID collision voltages (15 V-27 V) were utilized for a better fragment coverage across the mass range. The same ion optics parameters used during broadband ESI-FT-ICR MS experiments were utilized for the MS/MS analysis. Six to eight segments of 60-100 MS/MS scans each were collected across the predefined m/z range using serial run mode acquisition. Tandem MS spectra of the DOM samples were collected at 2 MW data acquisition size (mass resolution of \sim 140k at 400 m/ z).

(–)ESI-TIMS-FT-ICR MS. A custom-built Solarix 7T ESI-TIMS-FT-ICR MS spectrometer with an infinity ICR cell (Bruker Daltonics Inc., MA) was utilized to obtain isomeric information for the precursor molecules included in the structural families. The ESI operating conditions were the same as for the ESI-FT-ICR MS analysis described above. Typical transmission operational parameters included funnel rf amplitude 220 peak-to-peak voltage (Vpp), capillary exit –100 V, deflector plate –90 V, skimmer1 –60 V, transfer line rf 350 Vpp, octupole rf amplitude 350 Vpp, and collision cell rf 1000 Vpp. Mass profiles of the four DOM samples were collected at 4 MW data acquisition size.

The principle of the separation of ions in the gas phase using TIMS-ESI-FT-ICR MS is described elsewhere. $^{36,49-51}$ Briefly, ions in the TIMS cartridge are held against a nitrogen flow using an electric field applied on the electrodes. In these settings, the drag force exerted by the moving gas is counteracted by the electric field force so that the ions can be spatially separated across the TIMS analyzer axis based on

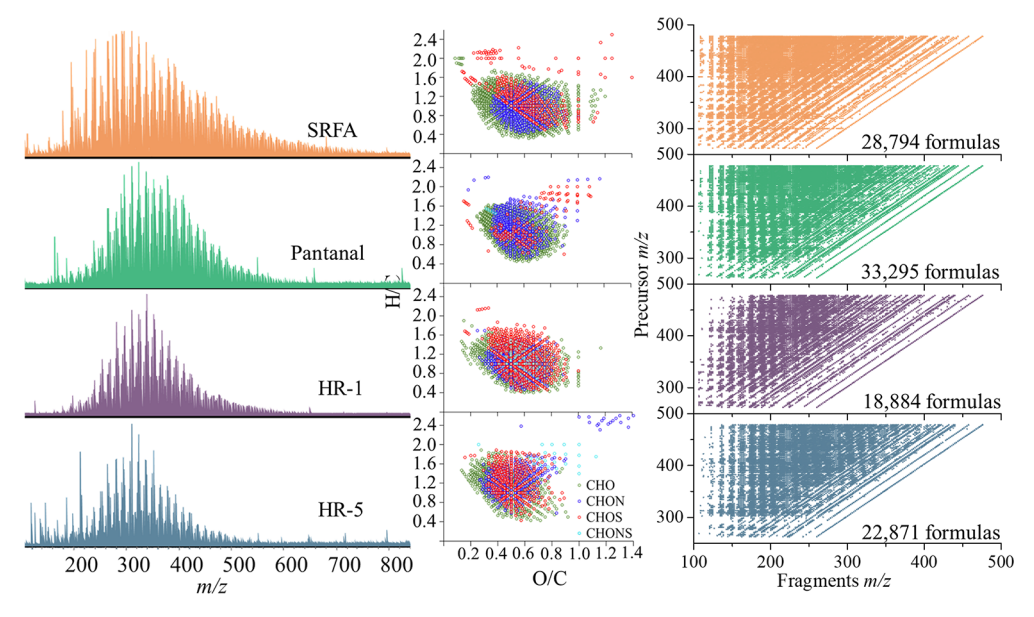


Figure 1. (–)ESI-FT-ICR MS spectra of the SRFA, Pantanal, HR-1, and HR-5 DOM samples (left panel), van Krevelen plots of the DOM samples highlighting the CHO, CHON, CHOS, and CHONS heteroatom classes (center panel), and 2D MS/MS plots obtained from the analysis of the DOM samples by the (–)ESI-FT-ICR CASI-CID MS/MS (right panel). Note that the number of chemical formulas indicated in the right panel for each DOM sample comprises the sum of precursors formulas obtained in both MS and MS/MS experiments, as well as fragment molecules assigned in more than 200 MS/MS spectra.

their ion mobility. $^{52-54}$ To improve the trapping efficiency of the TIMS cell, ions are radially confined using a quadrupolar RF field. The ion mobility, K_0 , of a charged molecule in a TIMS cell can be described by eq 1

$$K_0 = \frac{v_g}{E} = \frac{A}{V_{clution} - V_{out}} \tag{1}$$

where v_g , E, A, $V_{elution}$, and V_{out} are the velocity of the gas, electric field, a calibration constant, elution voltage, and tunnel out voltage, respectively.

Ion-neutral collisional cross sections (CCS (Ω, \mathring{A}^2)), which are an indication of the size and shape of the charged molecules, can be calculated from K_0 using the Mason–Schamp equation (eq 2)

$$\Omega = \frac{(18\pi)^{1/2}z}{16(k_{\rm B}T)^{1/2}} \left(\frac{1}{m_i} + \frac{1}{m_b}\right)^{1/2} \frac{1760T}{K_0 P273.15N^*}$$
(2)

where z is the charge of the ion, $k_{\rm B}$ is the Boltzmann constant, N^* is the number density, and m_i and m_b are the masses of the ion and bath gas, respectively (McDaniel and Mason 1973).

In-house software written in National Instruments LabVIEW synchronized with the FTMS control acquisition software was used for controlling the TIMS cartridge. The collection of IMS frames was conducted in the oversampling mode previously described by our group. 12,36,44,49 Nitrogen gas at ca. 300 K was employed as the bath gas, and pressures P1 = 2.4 mbar, P2 = 1.0 mbar, and a 220 Vpp rf were also utilized. The TIMS cell was operated using a simultaneous fill/trap sequence synchronized with the accumulation during detect mode of the FTMS control software. A voltage difference of 4 V across the ΔE gradient and a 0.2 V stepping scan function across the total 100 V ΔV range were utilized. A maximum of 1,000 IMS scans was collected per mass spectrum.

Data Processing. Data was processed using Data Analysis (v. 5.2, Bruker Daltonics, CA), and the plots were created using OriginPro 2016 (Originlab Co., MA). The assignment of

chemical formulas was conducted using Composer software (version 1.0.6, Sierra Analytics, CA, USA) and confirmed with Data Analysis (version 5.2, Bruker Daltonics). The assignment was validated by the lowest formula errors, the confirmation of isotopologues, and the removal of assigned peaks belonging to classes with only a few sparsely scattered members. Theoretical formula constraints of $C_{4-50}H_{4-100}N_{0-3}O_{0-25}S_{0-2}$, S/N > 3, m/z range 100–800, error < 1 ppm, $0 < O/C \le 1.2$, $0.3 \le H/C \le 1.2$ 2.5, and DBE-O $\leq 10^{55}$ were considered. An internal walking recalibration using the oxygen homologous series (O_4-O_{20}) was performed in Composer software. An average recalibration error < 200 ppb in the mass range 200-700 Da was obtained for the MS spectra of the four DOM samples. The fragment spectra were internally calibrated using a list of exact masses of fragment ions obtained from regularly occurring neutral losses in DOM and their combinations. 10,11

Input files containing the accurate mass of assigned peaks from MS₂ and MS₁, the isolated nominal mass, the ion abundance, and the assigned chemical formulas were processed using our developed in-house Python code Graph-DOM. 45,46 Briefly, ordered fragmentation pathways considering multiples of CH₄, O, H₂O, CO, CH₂O, CH₄O, and CO₂ neutral losses and with 1 mDa tolerance error were computed using Graph-DOM. Families of structurally related precursors were identified using a conceptual model based on *de novo* matching of fragmentation pathways. 45,46 Networks of DOM structurally interconnected precursors belonging to the structural families were created using Cytoscape v.3.82.56 Briefly, a structural network is built by interconnecting DOM family members based on neutral losses correlated with structural functionalities. A list of precursor molecules found in structural families is imported into Cytoscape software and defined as nodes. The structural functionalities correlated with neutral loss differences among precursors in a family are imported as network edges. A comparison of the structural families obtained for each DOM sample was conducted using new functionalities added to *Graph-DOM.* For this purpose, precursor molecules forming a

family were concatenated and defined as mathematical sets. Common families across the four DOM samples were identified by intersecting (\cap) all sets. Unique families to each sample were determined by subtracting the union (\cup) of three of the family sets from the remaining one. For example, unique structural families to the SRFA sample were determined by subtracting the union of Pantanal, HR-1, and HR-5 sets from the SRFA set.

Isomeric information for the precursor molecules of the structural was obtained from (-) ESI-TIMS-FT-ICR MS. TIMS profiles of the precursor formulas were extracted using Data Analysis (v. 5.2, Bruker Daltonics, City, CA, USA). The ion mobility spectra were externally calibrated using the reported ion mobilities of the Agilent Tuning Mix calibration standard.⁵⁷ Extracted ion mobility profiles for each chemical formula were deconvoluted using the custom-built Software Assisted Molecular Elucidation (SAME) package written in Python v3.7.3. The SAME package relies on noise removal, mean gap filling, asymmetric least-squares smoothing for baseline correction, continuous wavelet transform (CWT)based peak detection (SciPy package), and Gaussian fitting with nonlinear least-squares functions. ⁵⁸ Common structural isomers for precursors belonging to the families shared by all DOM samples were filtered by concatenating CCS values with chemical formulas. The same mathematical set approach described above for the identification of common and unique families was utilized for the identification of common structural isomers across DOM samples sharing the same structural families.

3. RESULTS AND DISCUSSION

The Graph-DOM approach utilizes accurate masses and chemical formulas from ultrahigh-resolution MS and MS/MS data to find structural similarities among DOM compounds based on their unique fragmentation pathways. In this work, we extended the capabilities of Graph-DOM by finding structural commonalities and dissimilarities among four DOM samples from different origins. Here, we generated neutral loss-based structural families in a data set that included precursor and fragment molecules detected in nearly 110 CIDfragmented nominal masses. The structural families represented as sequences of structurally connected chemical formulas are further compared to one another to generate common and unique chemical fingerprints across DOM samples. Finally, the interconnections of precursors molecules in DOM families are described in the form of networks using Cytoscape software.

The broadband (-)ESI-FT-ICR MS analysis of SRFA, Pantanal, HR-1, and HR-5 DOM samples resulted in the typical unimodal distribution of signals centered at \sim 340 m/z(Figure 1, left panel) The SRFA, Pantanal, and HR-1 samples, all with a strong association with a wetland source, showed a high chemical diversity with an average of 2920 chemical formulas assigned in the mass range $100-800 \, m/z$. On the other hand, HR-5, the estuarine DOM sample, showed a less chemically diverse fingerprint (<2000 chemical components). The distribution of heteroatoms classes across samples showed that the CHO class (58%) dominates over the CHON (19%), CHOS (12%), and CHONS (1%) classes (Table S1), in good agreement with previous reports of wetland samples. Over 30% more CHO components were found for SRFA and Pantanal samples compared to HR-1 and HR-5. Moreover, HR-1 and HR-5 exhibited ~10% more enriched CHON and

CHOS signatures than SRFA and Pantanal DOMs. This heteroatom pattern comparison provides a first level description of DOM signatures at the molecular level.

The DOM compositional representation in the van Krevelen space showed the preponderance of lignin-like and tannins-like components (Figure 2, center panel). Nevertheless, it should

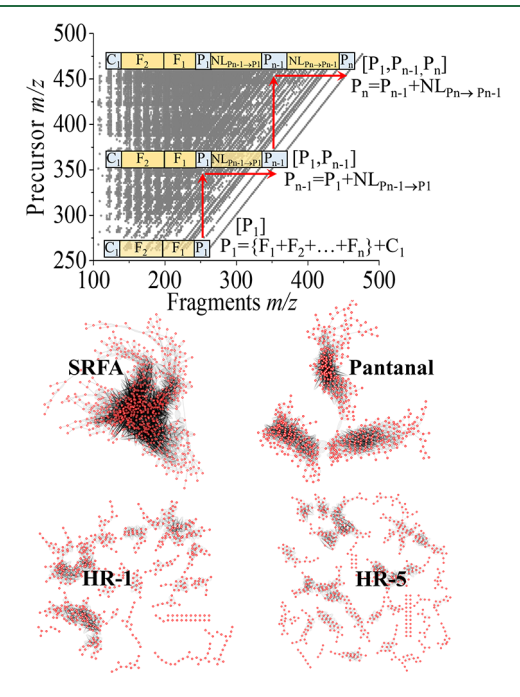


Figure 2. Schematic representation of Graph-DOM models used for identifying structural families (top panel) in a DOM sample. Cytoscape networks of structurally interconnected precursors of the SRFA, Pantanal, HR-1, and HR-5 DOM samples (bottom panel).

be clearly noted that these structural-like assignments are only indicative since they are solely based on chemical composition. A further structural comparison among DOM samples was conducted using neutral loss fragmentation patterns.

Inspection of the 2D MS/MS maps for the CHO class showed a similar pattern of typical neutral loss lines (i.e., $\rm H_2O$, $\rm CH_4O$, $\rm CH_2O$, and $\rm CO_2$ losses) and their multiples across the DOM samples (Figure 1, right panel). The fragment assignment of over 200 MS/MS spectra per DOM sample evidenced a higher structural diversity for the CHO class of SRFA and Pantanal samples (>10,000 fragment + precursor chemical formulas) compared with HR-1 and HR-5 samples. While this information was clearly uncovered by the CASI-CID MS/MS experiments, it was hindered at the MS1 level since HR-1 and HR-5 samples contained even more precursor molecules than SRFA and Pantanal samples (Table S1).

Examination of isolated mass signals at nominal mass 365 and their corresponding MS2 profiles (Figure S1) revealed that all DOM samples yielded a similar MS/MS fragmentation pattern with characteristic fragments to each DOM sample. A higher number of neutral losses was observed for SRFA and Pantanal samples compared with HR-1 and HR-5. Neutral losses are typically associated with structural functionalities. We interpret these results as that SRFA and Pantanal DOM samples have a larger structural diversity than HR-1 and HR-5 DOM samples.

The Graph-DOM schematics for the determination of structural families per DOM sample are visualized in Figure

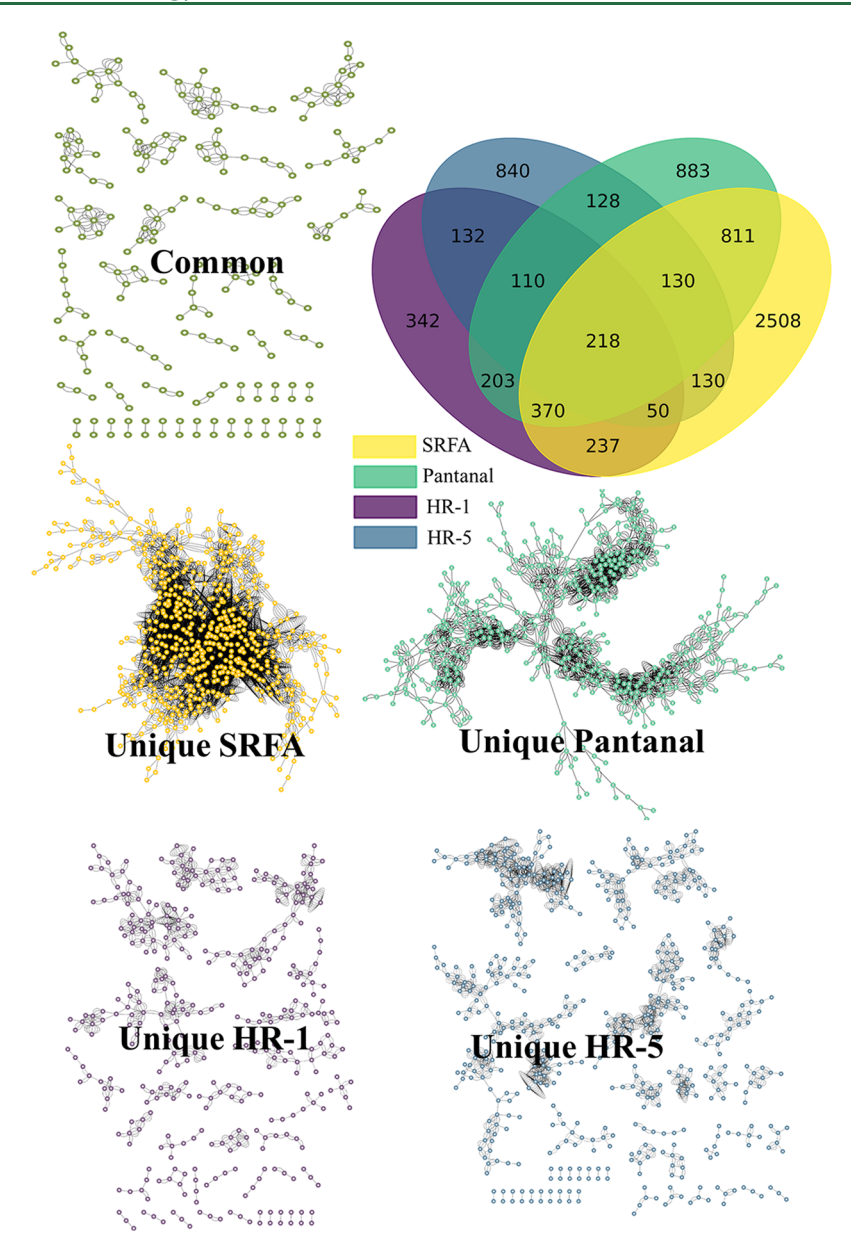


Figure 3. Venn diagram showing common structural families across DOM samples and unique families to SRFA, Pantanal, HR-1, and HR-5 determined by the comparison of families using Graph-DOM (top right panel). Cytoscape structural networks of common families found across the DOM samples (top left panel) and unique families to each sample (bottom).

2 (top panel). When applied to the CHO class, near 2-fold more fragmentation pathways were obtained for SRFA and Pantanal samples in comparison to HR-1 and HR-5 (Figure S2 top panel). In particular, SRFA and HR-1 exhibited the highest (10⁸) and lowest (10⁶) number of pathways, respectively. The number of structural families showed a similar trend across the DOM samples: SRFA > Pantanal > HR-5 > HR-1. An average family size distribution with 4–5 precursors was observed across all DOM samples (Figure S2 center panel); up to seven family members were found only for SRFA as an indication of its higher structural complexity.

Inspection of the CHO families showed that the top precursor (highest m/z) within a family for the Pantanal and HR-5 families showed 6–10 oxygens when compared with the SRFA and HR-1 structural families with over >12 oxygens (Figure S2 bottom). These results are in good agreement with previous reports where a higher structural diversity has been

associated with a higher number of oxygens. ⁴⁵ In particular, the SRFA higher structural diversity is exemplified by the larger family sizes (up to 7 precursors) and top family precursors with up to 15 oxygens. The Graph-DOM method resulted in being effective for the identification of structural commonalities and dissimilarities across DOMs. Further interpretation of the structural families can provide insight toward the correlation between DOC, DOM source, and biogeochemical transformations, among others. ¹¹

The observation of a single complex interconnected cluster of DOM components in the Cytoscape structural network of SRFA is consistent with its higher structural complexity (Figure 2, bottom panel). Although Pantanal's structural network (three interconnected clusters) looks slightly different than SRFA's network, they both shared similar interconnection complexities. The scattered clusters observed for HR-1 and HR-5 indicate that these two samples are structurally more

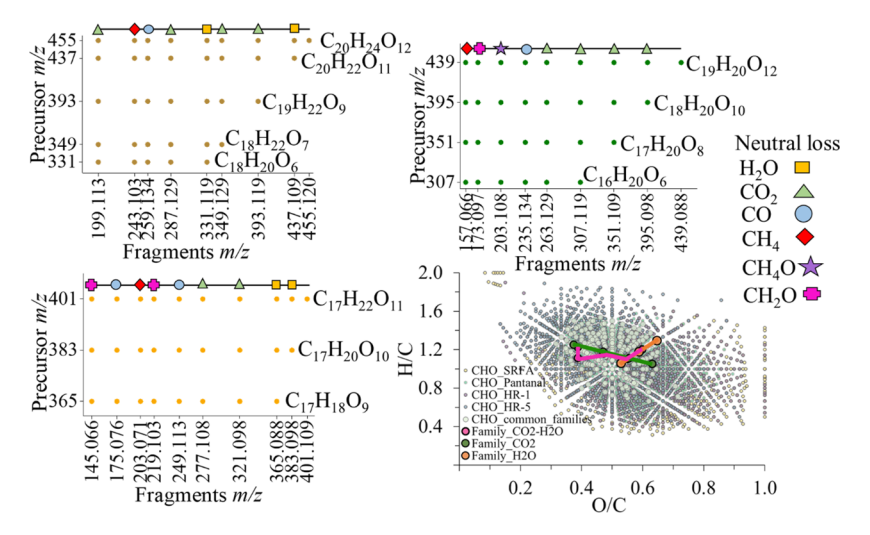


Figure 4. Representation of three common CHO families. The $H_2O-CO_2-CO_2-H_2O$ (top left), $CO_2-CO_2-CO_2$ (top right), and H_2O-H_2O (bottom left) families are depicted with one homologous fragmentation pathway in the form of 2D MS/MS fragments m/z vs precursor m/z plots. A van Krevelen plot (bottom right) showcases the compositional pattern of the CHO class components from the SRFA, Pantanal, HR-1, and HR-5 samples, the CHO precursors from the structural families shared by all DOM samples, and the three selected structural families.

similar between each other and less complex than Pantanal and SRFA, respectively. The structural similarity of HR-1 and HR-5 could be explained by the fact that both samples belong to the same ecosystem (Harney River, Everglades) along a transition from mainly Everglades DOM to additional sources from mangrove swamps and some marine inputs (particularly for HR-5). The differences observed in the structural networks (HR-1 contains more complex clusters than HR-5.) evidence different DOM biogeochemical transformations and different inputs associated with the different mangrove and marine derived inputs (Figure S3). While this comparison of structural families was limited to the CHO class (most abundant class), further inspection of other heteroatom classes can provide additional information.

The Graph-DOM provided a list of structural families for each DOM sample. A comparison of the structural families is shown using a Venn diagram in Figure 3. Note that the comparison using family sets (Figure S4) enabled the identification of common and unique structural families across the four DOM samples. Results showed that 8% of the CHO families across the four DOM samples are common; that is, over 200 families of structurally related CHO precursors are ubiquitous across distinctive aquatic environments.

The number of unique structural CHO families from the four DOM samples follows the same observed trend as the one from the number of fragmentation pathways and number of families (SRFA > Pantanal > HR-5 > HR-1). A high structural complexity of SRFA (>2500 unique families) and a high similarity with the Pantanal sample (>800 shared families) were observed. The Cytoscape structural network of the 218 CHO families common to all DOM samples showed a pattern of disconnected multiclusters (Figure 3 bottom panel). The lack of connectivity among structural families common to all samples could be associated with a lower structural diversity of HR-1 and HR-5 families compared to SRFA and Pantanal. We interpret these results as dissimilar input sources and transformational processes across aquatic environments. A closer look at the network of intersected families of SRFA and Pantanal but excluding both HR-1 and HR-5 families (Figure S5) confirmed the structural similarities of both SRFA and Pantanal samples. The exclusion of SRFA and Pantanal CHO

families from the intersection of HR-1 and HR-5 CHO families resulted in a network characterized by structural interconnections that resembles the ones obtained for the Everglades ecosystem (Figure S5 right). These results showed that the Graph-DOM method is effective for the determination of structural fingerprints associated with a DOM origin.

Inspection of the compositional characteristics of the CHO precursors within the common CHO families showed transformational processes associated with hydration and carboxylation steps. Three examples of common CHO structural families involving hydroxylic (H2O loss) and carboxylic (CO₂ loss) structural transitions among precursors are depicted in Figure 4. These transitions can be viewed as both synthetic and degradation pathways that illustrate some of complex biogeochemical mechanisms involved in DOM structural transformation. Although the molecular transformations resulting from CID fragmentation may be different than the ones triggered by enzymatically driven microbial processing, several studies have shown some interesting similarities in their pathways. For example, decarboxylation (CO2 neutral loss during CID) has been recognized as a biodegradation mechanism of tannins⁶⁰ and a fundamental reaction pathway of DOM photooxidation.^{61,62} Moreover, demethoxylation pathways, correlated with CH₄O neutral losses, have been previously reported during degradation of lignin, a potential DOM component. 63-65 The absence of methoxy (CH₄O loss)-based transformational processes in the common CHO structural families suggests that the mechanisms triggering the addition/subtraction of this functionality are characteristic to certain aquatic ecosystems. Examination of the neutral loss sequences among precursors in the families (data not shown) evidenced that at least one methoxy moiety was found in ~50% of both SRFA and Pantanal structural families. In contrast, lower abundance of this functionality was observed across HR-1 (<7%) and HR-5 (<3%) structural families, thus confirming the similarities between SRFA/ Pantanal and HR-1/HR-5 pairs at the structural level. Interestingly, the replacement of methoxy functional groups with phenolic hydroxyl groups has been previously linked to biodegradation of highly methoxylated lignin. 65-67 Therefore, transformation mechanisms involving methoxy moieties may

be constrained in estuarine systems (HR-1/HR-5) due to extensive upstream lignin biodegradation.

The three examples of common families superimposed on a van Krevelen plot (Figure 4) revealed continuous (orange and green) and discontinuous (pink) lines describing potential transformational pathways. These patterns illustrate that, in the context of our study (selected samples, conceptual model, and experimental setup), a set of constrained reactions pathways involving only addition/subtraction of hydroxyl and carboxylic moieties could be responsible for the ubiquitous pool of DOM structures across aquatic environments.

Complementary structural information can be derived from the use of mobility (TIMS) and neutral loss (CASI-CID FT-ICR MS/MS) experiments. A model describing the integration of the precursor isomeric information and neutral loss-based family identification is described in Figure S6. Briefly, the list of unique precursor formulas from the shared families was tagged with the isomeric information ($^{\rm TIMS}CCS_{\rm N2}$ values) from each DOM sample. The comparison of the new sets enabled the identification of common and unique precursor isomers shared by the common structural families (see the Venn diagram in Figure 5 top). A total of 450 isomeric precursors were shared by the common CHO structural families. Up to 4 isomers and an average of two isomeric species were found for precursors in the common families. Interestingly, the number of unique isomers found across precursors from common families

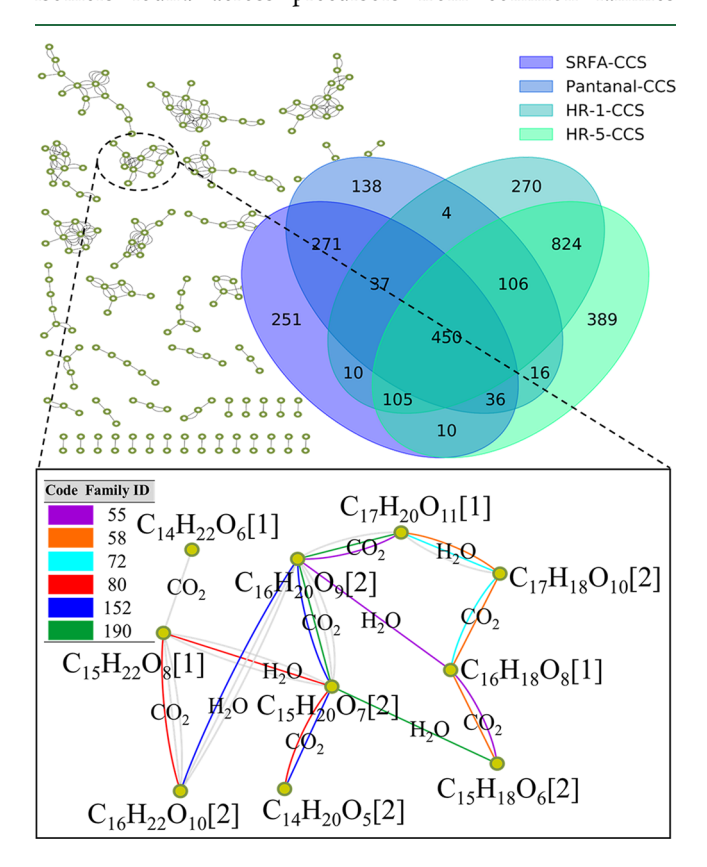


Figure 5. Venn diagram describing common and unique isomers for the precursors of the families shared by all DOM samples (top). Section of the structural network of families common to all samples (bottom) highlighting the interconnected precursor formulas (nodes), the family IDs (color code), the neutral based functionalities (edge label), and the number of common isomers across DOM samples per precursor (numbers in brackets). Note that gray lines are associated with other not labeled shorter families.

exhibited a decreasing trend in the order HR-5 > HR-1 > SRFA > Pantanal. These differences in isomeric content among common precursors could be one of the possible explanations behind the dissimilarities observed between the structural families of SRFA/Pantanal and HR-1/HR-5 pairs. However, it should be noted that the isomeric diversity provided in this study is a lower estimate; ¹² that is, mobility unresolved isomers should be accounted for.

An expanded view of a cluster from the network of common CHO families shows intraconnections of up to four precursors within a family (colored lines) and the complex interconnection among all families (Figure 5 bottom). The layer of isomeric information added on top of the family domain shows the presence of up to two isomers per precursor (number in brackets). In our previous report, 45 we suggested that the lines interconnecting two precursors in a network could be an indication of isomeric diversity based solely on the neutral loss information. A closer look at the expanded network on the bottom of Figure 5 reveals differences between the number of isomers estimated based on a neutral loss model (colored + gray lines) and mobility separation (number in brackets). For example, at least four isomers can be estimated for the C₁₅H₂₀O₇ precursor based on its CO₂ loss interconnections with C₁₆H₂₀O₉. On the other hand, the estimated lower number of isomers for C₁₅H₂₀O₇ based on the SAME fitting was two. Considering the potential ambiguities and shortcomings of each approach, the results are remarkable. Further integration of data using the chemical formula mobility selected MS/MS analytical workflow will be helpful in providing a training set of DOM unambiguous fragmentation information that can be incorporated in a machine learning algorithm.44

The results presented in this study show the potential of data mining of ultrahigh-resolution neutral loss fragmentation patterns using the Graph-DOM method in the description of DOM transformational networks at the molecular level. The role of the isomeric diversity at the molecular level was successfully integrated for the first time with the structural family description. The application of this methodology to DOM from different aquatic ecosystems allowed for the identification of common and unique DOM transformational networks. For the first time, evidence of common transformational processes is provided across these DOM samples. Future studies including samples of DOM photo/biodegradation experiments and samples along salinity transects could provide further insights into the DOM composition and correlation between the chemical components. All the Graph-DOM functionalities developed and described in this paper are freely accessible at https://github.com/Usman095/Graph-DOM.

ASSOCIATED CONTENT

Data Availability Statement

The updated Graph-DOM code along with the input files and web-based Cytoscape networks for each DOM sample are available at https://github.com/Usman095/Graph-DOM/tree/main/input. TIMS-FT-ICR MS and CASI-CID raw data for each DOM sample is freely accessible at https://doi.org/10.34703/gzx1-9v95/CLVLK6.

Solution Supporting Information

The Supporting Information is available free of charge at https://pubs.acs.org/doi/10.1021/acs.est.2c04715.

Figure S1, expanded view of precursor molecules (m/z)365) of SRFA, Pantanal, HR-1, and HR-5 DOM samples isolated in quadrupole $(\Delta m/z = 1)$ and their corresponding ESI (-) FT-ICR CID MS/MS spectra; Figure S2, number of precursors, core and intermediate fragments covered by Graph-DOM code, distribution of number of families per family size, and families per oxygen class of uppermost precursor for CHO class of each DOM sample; Figure S3, map of sampling point location for HR-1 and HR-5 samples in the Harney River, Florida, Everglades; Figure S4, conceptual model based on mathematical sets used for comparison of DOM structural families across samples; Figure S5, structural networks from intersection of pair SRFA/ Pantanal excluding HR-1&HR-5 and pair HR-1/HR-5 excluding SRFA&Pantanal; Figure S6, conceptual model developed for comparison of concatenated formulas and CCS values of common families across samples; and Table S1, summary of compositional information obtained for SRFA, Pantanal, HR-1, and HR-5 samples using ESI-FT-ICR MS (PDF)

AUTHOR INFORMATION

Corresponding Author

Francisco Fernandez-Lima — Department of Chemistry and Biochemistry, Florida International University, Miami, Florida 33199, United States; Biomolecular Sciences Institute, Florida International University, Miami, Florida 33199, United States; orcid.org/0000-0002-1283-4390; Email: fernandf@fiu.edu

Authors

Dennys Leyva — Department of Chemistry and Biochemistry, Florida International University, Miami, Florida 33199, United States

Muhammad Usman Tariq – School of Computing and Information Science, Florida International University, Miami, Florida 33199, United States

Rudolf Jaffé — Institute of Environment and Department of Chemistry and Biochemistry, Florida International University, Miami, Florida 33199, United States;
occid.org/0000-0001-6153-248X

Fahad Saeed — School of Computing and Information Science, Florida International University, Miami, Florida 33199, United States

Complete contact information is available at: https://pubs.acs.org/10.1021/acs.est.2c04715

Author Contributions

The manuscript was written through contributions of all authors. All authors have given approval to the final version of the manuscript.

Notes

The authors declare no competing financial interest.

ACKNOWLEDGMENTS

This work was supported by the National Science Foundation Division of Chemistry, under CAREER award CHE-1654274, with cofunding from the Division of Molecular and Cellular Biosciences to F.F.L. D.L. acknowledges the fellowship provided by the National Science Foundation award (HRD-1547798) to Florida International University as part of the

Centers for Research Excellence in Science and Technology (CREST) Program. D.L. also would like to acknowledge John Kominoski, Edward Castañeda, Ryan Bremen, and Kenny Anderson from the Ecosystem Ecology Laboratory at Florida International University (FIU) for their field and laboratory support, as well as Michael G. Rugge from the Institute of Environment at FIU for his help on generating the map. This is contribution number 1524 from the Institute of Environment at Florida International University. This material was developed in collaboration with the Florida Coastal Everglades Long Term Ecological Research program under the National Science Foundation Grant No. DEB-2025954. The authors acknowledge the personnel of the Advance Mass Spectrometry Facility at Florida International University as well as David Stranz and Sierra Analytics, Inc. for their support with the Composer software.

REFERENCES

- (1) Chantigny, M. H. Dissolved and water-extractable organic matter in soils: a review on the influence of land use and management practices. *Geoderma* **2003**, *113* (3), 357–380.
- (2) Tremblay, L.; Gagné, J.-P. Organic matter distribution and reactivity in the waters of a large estuarine system. *Marine Chemistry* **2009**, *116* (1), 1–12.
- (3) Ridgwell, A.; Arndt, S.Chapter 1 Why Dissolved Organics Matter: DOC in Ancient Oceans and Past Climate Change. In *Biogeochemistry of Marine Dissolved Organic Matter*, 2nd ed.; Hansell, D. A., Carlson, C. A., Eds.; Academic Press: Boston, 2015; pp 1–20, DOI: 10.1016/B978-0-12-405940-5.00001-7.
- (4) Moran, M. A.; Kujawinski, E. B.; Stubbins, A.; Fatland, R.; Aluwihare, L. I.; Buchan, A.; Crump, B. C.; Dorrestein, P. C.; Dyhrman, S. T.; Hess, N. J.; Howe, B.; Longnecker, K.; Medeiros, P. M.; Niggemann, J.; Obernosterer, I.; Repeta, D. J.; Waldbauer, J. R. Deciphering ocean carbon in a changing world. *Proc. Natl. Acad. Sci. U. S. A.* 2016, 113 (12), 3143–3151.
- (5) Lønborg, C.; Carreira, C.; Jickells, T.; Álvarez-Salgado, X. A. Impacts of Global Change on Ocean Dissolved Organic Carbon (DOC) Cycling. Frontiers in Marine Science 2020, 7, 466.
- (6) Fakhraee, M.; Tarhan, L. G.; Planavsky, N. J.; Reinhard, C. T. A largely invariant marine dissolved organic carbon reservoir across Earth's history. *Proc. Natl. Acad. Sci. U. S. A.* **2021**, *118* (40), No. e2103511118.
- (7) Wagner, S.; Jaffé, R.; Cawley, K.; Dittmar, T.; Stubbins, A. Associations Between the Molecular and Optical Properties of Dissolved Organic Matter in the Florida Everglades, a Model Coastal Wetland System. *Frontiers in Chemistry* **2015**, *3*, *66*.
- (8) Osterholz, H.; Kirchman, D. L.; Niggemann, J.; Dittmar, T. Environmental Drivers of Dissolved Organic Matter Molecular Composition in the Delaware Estuary. *Frontiers in Earth Science* **2016**, *4*, 95.
- (9) Hertkorn, N.; Harir, M.; Cawley, K. M.; Schmitt-Kopplin, P.; Jaffé, R. Molecular characterization of dissolved organic matter from subtropical wetlands: a comparative study through the analysis of optical properties, NMR and FTICR/MS. *Biogeosciences* **2016**, *13* (8), 2257–2277.
- (10) Zark, M.; Christoffers, J.; Dittmar, T. Molecular properties of deep-sea dissolved organic matter are predictable by the central limit theorem: Evidence from tandem FT-ICR-MS. *Marine Chemistry* **2017**, 191, 9–15.
- (11) Zark, M.; Dittmar, T. Universal molecular structures in natural dissolved organic matter. *Nat. Commun.* **2018**, 9 (1), 3178.
- (12) Leyva, D.; Tose, L. V.; Porter, J.; Wolff, J.; Jaffé, R.; Fernandez-Lima, F. Understanding the structural complexity of dissolved organic matter: isomeric diversity. *Faraday Discuss.* **2019**, 218 (0), 431–440. (13) Xu, W.; Gao, Q.; He, C.; Shi, Q.; Hou, Z.-Q.; Zhao, H.-Z. Using ESI FT-ICR MS to Characterize Dissolved Organic Matter in

- Salt Lakes with Different Salinity. Environ. Sci. Technol. 2020, 54 (20), 12929–12937.
- (14) Asmala, E.; Massicotte, P.; Carstensen, J. Identification of dissolved organic matter size components in freshwater and marine environments. *Limnology and Oceanography* **2021**, *66* (4), 1381–1393.
- (15) He, D.; Li, P.; He, C.; Wang, Y.; Shi, Q. Eutrophication and watershed characteristics shape changes in dissolved organic matter chemistry along two river-estuarine transects. *Water Res.* **2022**, *214*, 118196.
- (16) Seidel, M.; Beck, M.; Riedel, T.; Waska, H.; Suryaputra, I. G. N. A.; Schnetger, B.; Niggemann, J.; Simon, M.; Dittmar, T. Biogeochemistry of dissolved organic matter in an anoxic intertidal creek bank. *Geochim. Cosmochim. Acta* **2014**, *140*, 418–434.
- (17) Antony, R.; Willoughby, A. S.; Grannas, A. M.; Catanzano, V.; Sleighter, R. L.; Thamban, M.; Hatcher, P. G.; Nair, S. Molecular Insights on Dissolved Organic Matter Transformation by Supraglacial Microbial Communities. *Environ. Sci. Technol.* **2017**, *51* (8), 4328–4337
- (18) Kim, S.; Kim, D.; Jung, M.-J.; Kim, S. Analysis of environmental organic matters by Ultrahigh-Resolution mass spectrometry—A review on the development of analytical methods. *Mass Spectrom. Rev.* **2022**, *41* (2), 352–369.
- (19) Zhang, Y.; Zhou, Y.; Shi, K.; Qin, B.; Yao, X.; Zhang, Y. Optical properties and composition changes in chromophoric dissolved organic matter along trophic gradients: Implications for monitoring and assessing lake eutrophication. *Water Res.* **2018**, *131*, 255–263.
- (20) O'Connor, J. A.; Lu, K.; Guo, L.; Rosenheim, B. E.; Liu, Z. Composition and lability of riverine dissolved organic matter: Insights from thermal slicing ramped pyrolysis GC–MS, amino acid, and stable isotope analyses. *Org. Geochem.* **2020**, *149*, 104100.
- (21) Gonsior, M.; Powers, L.; Lahm, M.; McCallister, S. L. New Perspectives on the Marine Carbon Cycle—The Marine Dissolved Organic Matter Reactivity Continuum. *Environ. Sci. Technol.* **2022**, *56* (9), 5371–5380.
- (22) Smith, D. F.; Podgorski, D. C.; Rodgers, R. P.; Blakney, G. T.; Hendrickson, C. L. 21 T FT-ICR Mass Spectrometer for Ultrahigh-Resolution Analysis of Complex Organic Mixtures. *Anal. Chem.* **2018**, 90 (3), 2041–2047.
- (23) Marshall, A. G.; Guan, S. Advantages of High Magnetic Field for Fourier Transform Ion Cyclotron Resonance Mass Spectrometry. *Rapid Commun. Mass Spectrom.* **1996**, *10* (14), 1819–1823.
- (24) Cooper, W. T.; Chanton, J. C.; D'Andrilli, J.; Hodgkins, S. B.; Podgorski, D. C.; Stenson, A. C.; Tfaily, M. M.; Wilson, R. M. A History of Molecular Level Analysis of Natural Organic Matter by FTICR Mass Spectrometry and The Paradigm Shift in Organic Geochemistry. *Mass Spectrom. Rev.* 2022, 41 (2), 215–239.
- (25) Berg, S. M.; Peterson, B. D.; McMahon, K. D.; Remucal, C. K. Spatial and Temporal Variability of Dissolved Organic Matter Molecular Composition in a Stratified Eutrophic Lake. *Journal of Geophysical Research: Biogeosciences* **2022**, *127* (1), e2021JG006550.
- (26) Seidel, M.; Vemulapalli, S. P. B.; Mathieu, D.; Dittmar, T. Marine Dissolved Organic Matter Shares Thousands of Molecular Formulae Yet Differs Structurally across Major Water Masses. *Environ. Sci. Technol.* **2022**, *56* (6), 3758–3769.
- (27) Lu, K.; Liu, Z. Molecular Level Analysis Reveals Changes in Chemical Composition of Dissolved Organic Matter From South Texas Rivers After High Flow Events. *Frontiers in Marine Science* **2019**, 6, 673.
- (28) Hertkorn, N.; Harir, M.; Schmitt-Kopplin, P. Nontarget analysis of Murchison soluble organic matter by high-field NMR spectroscopy and FTICR mass spectrometry. *Magn. Reson. Chem.* **2015**, 53 (9), 754–768.
- (29) Hertkorn, N.; Harir, M.; Koch, B. P.; Michalke, B.; Schmitt-Kopplin, P. High-field NMR spectroscopy and FTICR mass spectrometry: powerful discovery tools for the molecular level characterization of marine dissolved organic matter. *Biogeosciences* **2013**, *10* (3), 1583–1624.

- (30) Harir, M.; Cawley, K. M.; Hertkorn, N.; Schmitt-Kopplin, P.; Jaffé, R. Molecular and spectroscopic changes of peat-derived organic matter following photo-exposure: Effects on heteroatom composition of DOM. *Science of The Total Environment* **2022**, 838, 155790.
- (31) Petras, D.; Koester, I.; Da Silva, R.; Stephens, B. M.; Haas, A. F.; Nelson, C. E.; Kelly, L. W.; Aluwihare, L. I.; Dorrestein, P. C. High-Resolution Liquid Chromatography Tandem Mass Spectrometry Enables Large Scale Molecular Characterization of Dissolved Organic Matter. Frontiers in Marine Science 2017, 4, 405.
- (32) Qi, Y.; Ma, C.; Chen, S.; Ge, J.; Hu, Q.; Li, S.-L.; Volmer, D. A.; Fu, P. Online Liquid Chromatography and FT-ICR MS Enable Advanced Separation and Profiling of Organosulfates in Dissolved Organic Matter. ACS ES&T Water 2021, 1 (8), 1975–1982.
- (33) Hawkes, J. A.; Patriarca, C.; Sjöberg, P. J. R.; Tranvik, L. J.; Bergquist, J. Extreme isomeric complexity of dissolved organic matter found across aquatic environments. *Limnology and Oceanography Letters* **2018**, 3 (2), 21–30.
- (34) Lu, K.; Li, X.; Chen, H.; Liu, Z. Constraints on isomers of dissolved organic matter in aquatic environments: Insights from ion mobility mass spectrometry. *Geochim. Cosmochim. Acta* **2021**, 308, 353–372.
- (35) Gao, Y.; Wang, W.; He, C.; Fang, Z.; Zhang, Y.; Shi, Q. Fractionation and molecular characterization of natural organic matter (NOM) by solid-phase extraction followed by FT-ICR MS and ion mobility MS. *Anal. Bioanal. Chem.* **2019**, *411*, 6343–6352.
- (36) Tose, L. V.; Benigni, P.; Leyva, D.; Sundberg, A.; Ramírez, C. E.; Ridgeway, M. E.; Park, M. A.; Romão, W.; Jaffé, R.; Fernandez-Lima, F. Coupling trapped ion mobility spectrometry to mass spectrometry: trapped ion mobility spectrometry—time-of-flight mass spectrometry versus trapped ion mobility spectrometry—Fourier transform ion cyclotron resonance mass spectrometry. *Rapid Commun. Mass Spectrom.* 2018, 32 (15), 1287–1295.
- (37) Powers, L. C.; Lapham, L. L.; Malkin, S. Y.; Heyes, A.; Schmitt-Kopplin, P.; Gonsior, M. Molecular and optical characterization reveals the preservation and sulfurization of chemically diverse porewater dissolved organic matter in oligohaline and brackish Chesapeake Bay sediments. Org. Geochem. 2021, 161, 104324.
- (38) Pan, Q.; Zhuo, X.; He, C.; Zhang, Y.; Shi, Q. Validation and Evaluation of High-Resolution Orbitrap Mass Spectrometry on Molecular Characterization of Dissolved Organic Matter. *ACS Omega* **2020**, *5* (10), 5372–5379.
- (39) Hawkes, J. A.; Dittmar, T.; Patriarca, C.; Tranvik, L.; Bergquist, J. Evaluation of the Orbitrap Mass Spectrometer for the Molecular Fingerprinting Analysis of Natural Dissolved Organic Matter. *Anal. Chem.* **2016**, *88* (15), 7698–7704.
- (40) Hertkorn, N.; Benner, R.; Frommberger, M.; Schmitt-Kopplin, P.; Witt, M.; Kaiser, K.; Kettrup, A.; Hedges, J. I. Characterization of a major refractory component of marine dissolved organic matter. *Geochim. Cosmochim. Acta* **2006**, *70* (12), 2990–3010.
- (41) Cortés-Francisco, N.; Caixach, J. Fragmentation studies for the structural characterization of marine dissolved organic matter. *Anal. Bioanal. Chem.* **2015**, 407 (9), 2455–2462.
- (42) LeClair, J. P.; Collett, J. L.; Mazzoleni, L. R. Fragmentation Analysis of Water-Soluble Atmospheric Organic Matter Using Ultrahigh-Resolution FT-ICR Mass Spectrometry. *Environ. Sci. Technol.* **2012**, *46* (8), 4312–4322.
- (43) Osterholz, H.; Niggemann, J.; Giebel, H.-A.; Simon, M.; Dittmar, T. Inefficient microbial production of refractory dissolved organic matter in the ocean. *Nat. Commun.* **2015**, 6 (1), 7422.
- (44) Leyva, D.; Jaffe, R.; Fernandez-Lima, F. Structural Characterization of Dissolved Organic Matter at the Chemical Formula Level Using TIMS-FT-ICR MS/MS. *Anal. Chem.* **2020**, 92 (17), 11960–11966.
- (45) Leyva, D.; Tariq, M. U.; Jaffé, R.; Saeed, F.; Lima, F. F. Unsupervised Structural Classification of Dissolved Organic Matter Based on Fragmentation Pathways. *Environ. Sci. Technol.* **2022**, *56* (2), 1458–1468.
- (46) Usman Tariq, M.; Leyva, D.; Lima, F. A. F.; Saeed, F.Graph Theoretic Approach for the Analysis of Comprehensive Mass-

- Spectrometry (MS/MS) Data of Dissolved Organic Matter. In 2021 IEEE International Conference on Bioinformatics and Biomedicine (BIBM); 2021; pp 3742-3746, DOI: 10.1109/ bibm52615.2021.9669289.
- (47) Li, Y.; Harir, M.; Lucio, M.; Kanawati, B.; Smirnov, K.; Flerus, R.; Koch, B. P.; Schmitt-Kopplin, P.; Hertkorn, N. Proposed Guidelines for Solid Phase Extraction of Suwannee River Dissolved Organic Matter. Anal. Chem. 2016, 88 (13), 6680-6688.
- (48) Dittmar, T.; Koch, B.; Hertkorn, N.; Kattner, G. A simple and efficient method for the solid-phase extraction of dissolved organic matter (SPE-DOM) from seawater. Limnology and Oceanography: Methods 2008, 6 (6), 230-235.
- (49) Benigni, P.; Fernandez-Lima, F. Oversampling Selective Accumulation Trapped Ion Mobility Spectrometry Coupled to FT-ICR MS: Fundamentals and Applications. Anal. Chem. 2016, 88 (14), 7404-7412.
- (50) Benigni, P.; Sandoval, K.; Thompson, C. J.; Ridgeway, M. E.; Park, M. A.; Gardinali, P.; Fernandez-Lima, F. Analysis of Photoirradiated Water Accommodated Fractions of Crude Oils Using Tandem TIMS and FT-ICR MS. Environ. Sci. Technol. 2017, 51 (11),
- (51) Benigni, P.; Porter, J.; Ridgeway, M. E.; Park, M. A.; Fernandez-Lima, F. Increasing Analytical Separation and Duty Cycle with Nonlinear Analytical Mobility Scan Functions in TIMS-FT-ICR MS. Anal. Chem. 2018, 90 (4), 2446-2450.
- (52) Fernandez-Lima, F.; Kaplan, D. A.; Suetering, J.; Park, M. A. Gas-phase separation using a trapped ion mobility spectrometer. International Journal for Ion Mobility Spectrometry 2011, 14 (2), 93-
- (53) Fernandez-Lima, F. A.; Kaplan, D. A.; Park, M. A. Note: Integration of trapped ion mobility spectrometry with mass spectrometry. Rev. Sci. Instrum. 2011, 82 (12), 126106.
- (54) Hernandez, D. R.; DeBord, J. D.; Ridgeway, M. E.; Kaplan, D. A.; Park, M. A.; Fernandez-Lima, F. Ion dynamics in a trapped ion mobility spectrometer. Analyst 2014, 139 (8), 1913-1921.
- (55) Herzsprung, P.; Hertkorn, N.; von Tümpling, W.; Harir, M.; Friese, K.; Schmitt-Kopplin, P. Understanding molecular formula assignment of Fourier transform ion cyclotron resonance mass spectrometry data of natural organic matter from a chemical point of view. Anal. Bioanal. Chem. 2014, 406 (30), 7977-7987.
- (56) Smoot, M. E.; Ono, K.; Ruscheinski, J.; Wang, P.-L.; Ideker, T. Cytoscape 2.8: new features for data integration and network visualization. *Bioinformatics* **2011**, 27 (3), 431–432.
- (57) Stow, S. M.; Causon, T. J.; Zheng, X.; Kurulugama, R. T.; Mairinger, T.; May, J. C.; Rennie, E. E.; Baker, E. S.; Smith, R. D.; McLean, J. A.; Hann, S.; Fjeldsted, J. C. An Interlaboratory Evaluation of Drift Tube Ion Mobility-Mass Spectrometry Collision Cross Section Measurements. Anal. Chem. 2017, 89 (17), 9048-9055.
- (58) Benigni, P.; Marin, R.; Sandoval, K.; Gardinali, P.; Fernandez-Lima, F. Chemical Analysis of Water-accommodated Fractions of Crude Oil Spills Using TIMS-FT-ICR MS. J. Visualized Exp. 2017, 121, No. 55352.
- (59) Cawley, K. M.; Yamashita, Y.; Maie, N.; Jaffé, R. Using Optical Properties to Quantify Fringe Mangrove Inputs to the Dissolved Organic Matter (DOM) Pool in a Subtropical Estuary. Estuaries and Coasts 2014, 37 (2), 399-410.
- (60) Bhat, T. K.; Singh, B.; Sharma, O. P. Microbial degradation of tannins - A current perspective. Biodegradation 1998, 9 (5), 343-357.
- (61) Xie, H.; Zafiriou, O. C.; Cai, W.-J.; Zepp, R. G.; Wang, Y. Photooxidation and Its Effects on the Carboxyl Content of Dissolved Organic Matter in Two Coastal Rivers in the Southeastern United States. Environ. Sci. Technol. 2004, 38 (15), 4113-4119.
- (62) Riedel, T.; Zark, M.; Vähätalo, A. V.; Niggemann, J.; Spencer, R. G. M.; Hernes, P. J.; Dittmar, T. Molecular Signatures of Biogeochemical Transformations in Dissolved Organic Matter from Ten World Rivers. Frontiers in Earth Science 2016, 4, 85.

(63) Khan, M. U.; Ahring, B. K. Lignin degradation under anaerobic digestion: Influence of lignin modifications -A review. Biomass and Bioenergy 2019, 128, 105325.

pubs.acs.org/est

- (64) Weng, C.; Peng, X.; Han, Y. Depolymerization and conversion of lignin to value-added bioproducts by microbial and enzymatic catalysis. Biotechnology for Biofuels 2021, 14 (1), 84.
- (65) Cui, L.; Wang, Z.; Zeng, Y.; Yang, N.; Liu, M.; Zhao, Y.; Zheng, Y. Lignin Biodegradation and Its Valorization. Fermentation 2022, 8 (8), 366.
- (66) Venkatesagowda, B. Enzymatic demethylation of lignin for potential biobased polymer applications. Fungal Biology Reviews 2019, 33 (3), 190-224.
- (67) Venkatesagowda, B.; Dekker, R. F. H. Enzymatic demethylation of Kraft lignin for lignin-based phenol-formaldehyde resin applications. Biomass Conversion and Biorefinery 2020, 10 (2), 203-225.

□ Recommended by ACS

Effect of Stoichiometry on Nanomagnetite Sulfidation

Mingjun Nie, Juan Liu, et al.

FEBRUARY 06, 2023

ENVIRONMENTAL SCIENCE & TECHNOLOGY

READ **Z**

Persisting Effects in Daphnia magna Following an Acute **Exposure to Flowback and Produced Waters from the Montney Formation**

Aaron Boyd, Tamzin A. Blewett, et al.

FEBRUARY 01, 2023

ENVIRONMENTAL SCIENCE & TECHNOLOGY

READ **C**

Water Ouality in Puerto Rico after Hurricane Maria: **Challenges Associated with Water Quality Assessments and Implications for Resilience**

Melanie Warren, Julie A. Korak, et al.

JANUARY 24, 2023

ACS ES&T WATER

RFAD 17

Co-Occurrence of Bromine and Iodine Species in US **Drinking Water Sources That Can Impact Disinfection Byproduct Formation**

Naushita Sharma, Paul Westerhoff, et al.

JANUARY 17, 2023

ENVIRONMENTAL SCIENCE & TECHNOLOGY

RFAD 🗹

Get More Suggestions >